Optimal Formation Reconfiguration of Satellites Under Attitude Constraints Using Only Thrusters

Yoshimura, Yasuhiro
Tokyo Metropolitan University

出版情報：Aerospace Science and Technology. 77, pp.449-457, 2018-06. Elsevier
バージョン：
権利関係：

Optimal Formation Reconfiguration of Satellites Under Attitude Constraints Using Only Thrusters

Yasuhiro Yoshimura[a,*]

[a] *Tokyo Metropolitan University, 6-6 Asahigaoka, Hino, Tokyo*

Abstract

An optimal formation reconfiguration method under the constraints of a satellite attitude with respect to an inertial frame is addressed. Both the satellite position and attitude are controlled by only two body-fixed thrusters for an in-plane maneuver. To tackle the underactuated control problem, an attitude controller for tracking reference accelerations is firstly derived on the basis of Lyapunov approach. This controller allows us to consider the attitude constraints as input directional constraints because the satellite attitude is controlled so that the thrust direction is coincide with the force direction required for the orbit transfer. Secondly, a formation reconfiguration method based on the Fourier series is used as the reference inputs, and boundary conditions that make the resulting input trajectory an ellipse are shown. Such elliptic input trajectory changes the input direction monotonically, which enables bounding it around an desired direction. The proposed underactuated-controller achieves a reconfiguration maneuver while keeping the satellite attitude within a range from a specified direction, and thus is useful when several thrusters of a satellite fail due to malfunctions. Finally, numerical simulation results validate the effectiveness of the proposed relocation method by comparing energy consumptions and bounded satellite attitude angles.

Keywords: Optimal reconfiguration, Attitude constraints, Formation flying, Thrusters

1. Introduction

Formation flying is one of promising technologies for space missions [1, 2, 3, 4], in which several satellites are orbiting on a close formation and controlled to keep their relative position and attitude to one another. The relative motion of a satellite, called "follower", with respect to a "leader" satellite have been discussed using linearized equations. The equations of motion of the follower in the proximity of the leader is expressed with Hill–Clohessy–Wiltshire (HCW) equations [5] for a circular orbit and Tschauner-Hempel equations [6] for an elliptic orbit. These linearized equations have periodic solutions and they are useful to design satellite formation relocation or rendezvous trajectories [7, 8, 9]. From a practical

*Corresponding author

Email address: yyoshi@tmu.ac.jp (Yasuhiro Yoshimura)

viewpoint, optimal trajectories to desired relative orbits should be designed to minimize energy or fuel consumption. In terms of energy optimality, Carter and Pardis [10] propose an optimal feedback controller for a rendezvous problem in a circular orbit under constraints of bounded thrusts. Palmer [11] analytically shows an optimal controller based on the Fourier series for relocating a follower satellite to a desired relative orbit. This method is extended to study analytical solutions for optimal formation reconfigurations under J_2 perturbation [12] as well as to derive an optimal controller for formation flying in an elliptic orbit [13]. For both energy and fuel optimizations, Xi and Li [14] show an optimal reconfiguration method in an elliptic orbit using a homotopy method. Though these methods enable optimal formation control, arbitrary magnitudes of accelerations are assumed available in any directions. This assumption implies that enough number of thrusters are equipped on satellites, and thus the prior controllers are not applicable when some thrusters have failed or a satellite equips a few number of thrusters.

Even if a follower satellite equips enough number of thrusters, the satellite attitude control throughout a reconfiguration maneuver is needed for practical mission requirements. Moreover, the satellite attitude depends on the thrust directions when only a few number of thrusters are available. In that case, the thrust directions must be oriented along desired directions by controlling the satellite attitude. This indicates that the requirements on the attitude angles can be equivalently considered as input directional constraints. Mitani and Yamakawa [15] show an optimal rendezvous method under thrust directional constraints with respect to a leader satellite. The optimal controller is based on a satisficing method [16] for keeping the thrust direction within an allowable area. The control method in [15] is further extended to an optimal controller [17] in terms of L_1 and L_2 optimizations of thruster accelerations by the use of a smoothing method. Guelman et al. [18] deal with a formation control under a single input constraint in a circular orbit. Recent research deals with position and attitude control of satellites in formation flying [19, 20, 21]. These studies, however, assume that the satellite attitude can be controlled arbitrarily. That is, the attitude dynamics of a follower satellite is not explicitly studied. Therefore the existing control methods may affect the attitude motion in the formation flying and are not applicable to the system in this paper.

This study aims to show an optimal formation reconfiguration method under a satellite attitude constraint with respect to an inertial frame. In the reconfiguration maneuver for in-plane motion, both the satellite position and attitude are controlled using only two thrusters. For such an underactuated satellite, its attitude angle must be controlled for generating thruster forces in desired directions. Thus this study firstly derives an attitude tracking controller using the thruster inputs on the basis of Lyapunov stability. The derived tracking controller reduces the reconfiguration problem under the attitude constraint to the one under a thrust directional constraint. Secondly, reference inputs for the tracking method is designed. Then, the conditions of the reference inputs to bound the thrust direction around desired one are discussed. The maximum bound of the attitude angle can be accurately estimated. Numerical simulation results verify the effectiveness of the proposed controller and the accuracy of the estimated bounds, and compare the energy consumptions. The proposed underactuated control method uses two thrusters for the reconfiguration maneuver

while keeping the satellite attitude in a certain region. The proposed method is useful and applicable for formation flying maneuvers under attitude constraints such as electric power generation with fixed solar array panels, coronagraph observations[3, 22] or communication with ground stations. The formation reconfiguration with only two thrusters also indicates that the number of actuators required for formation flying can be reduced and is useful when several thrusters of a satellite fail due to malfunctions.

This paper is organized as follows. Section 2 denotes the relative equations of a follower satellite in a near-circular orbit and their analytical solutions. Modal equations are also shown to simplify the interpretation of the reconfiguration problem. Section 3 describes an optimal reconfiguration method and its boundary conditions to orient the satellite attitude along a desired direction. Furthermore, an initial input direction and the estimation of the attitude bound are analyzed. Finally, some numerical simulation results are shown to verify the effectiveness of the proposed method in Section 4, and Section 5 concludes this paper.

2. Problem Formulation

2.1. Hill–Clohessy–Wiltshire equations

The relative motion of a follower satellite is described in a leader-fixed frame. In the leader-fixed coordinate system, x-axis lies in the radial direction from the Earth, z-axis points to the orbital momentum vector of the leader, and y-axis completes the right-handed frame. Since the cross-track motion along the z-axis is decoupled from the in-plane motion, this study considers a formation reconfiguration in the x–y plane. If cross-track motion exists, the translational and rotational motion along the z-axis should be firstly controlled so that the proposed method in this paper can be applied. The in-plane equations of motion are written as

$$\ddot{x} = 2\Omega\dot{y} + \Omega^2 (R_l + x) - \frac{\mu (R_l + x)}{\left((R_l + x)^2 + y^2 + z^2\right)^{\frac{3}{2}}} + u_x \tag{1}$$

$$\ddot{y} = -2\Omega\dot{x} + \Omega^2 y - \frac{\mu y}{\left((R_l + x)^2 + y^2 + z^2\right)^{\frac{3}{2}}} + u_y \tag{2}$$

where Ω, R_l, and μ are the orbital rate of the leader satellite, the orbital radius of the leader, and the gravitational constant, respectively. The variables (x, y, z) and (u_x, u_y) denote the relative position of the follower and external accelerations. Although practical disturbances such as atmospheric drag and/or solar radiation pressure should be considered in the external accelerations, this study ignores these effects to simplify the simultaneous control of the relative position and attitude. The extension of the proposed method to the motion under the disturbances will be studied in future works.

Assuming that the orbital radius of the leader is much larger than the distance between

the leader and follower, we obtain linearized equations, i.e., HCW equations [5] as

$$\frac{\mathrm{d}}{\mathrm{d}t}\begin{bmatrix} \Omega x \\ \dot{x} \\ \Omega y \\ \dot{y} \end{bmatrix} = \begin{bmatrix} 0 & \Omega & 0 & 0 \\ 3\Omega & 0 & 0 & 2\Omega \\ 0 & 0 & 0 & \Omega \\ 0 & -2\Omega & 0 & 0 \end{bmatrix} \begin{bmatrix} \Omega x \\ \dot{x} \\ \Omega y \\ \dot{y} \end{bmatrix} + \begin{bmatrix} 0 & 0 \\ 1 & 0 \\ 0 & 0 \\ 0 & 1 \end{bmatrix} \begin{bmatrix} u_x \\ u_y \end{bmatrix} \tag{3}$$

$$\Rightarrow \dot{\boldsymbol{x}} = A\boldsymbol{x} + B\boldsymbol{u}_{xy} \tag{4}$$

Note that the variables x and y in the state vector $\boldsymbol{x}$ are multiplied by the orbital rate Ω to simplify analytical solutions shown in the followings.

The analytic solutions of the HCW equations with no external forces, i.e., homogeneous solutions, are described as follows.

$$\boldsymbol{x}_h(t) = \Phi(t)\,\boldsymbol{x}_i \tag{5}$$

where

$$\Phi(t) := \begin{bmatrix} 4 - 3c_\Omega & s_\Omega & 0 & 2(1 - c_\Omega) \\ 3s_\Omega & c_\Omega & 0 & 2s_\Omega \\ 6(s_\Omega - \Omega t) & -2(1 - c_\Omega) & 1 & 4s_\Omega - 3\Omega t \\ -6(1 - c_\Omega) & -2s_\Omega & 0 & -3 + 4c_\Omega \end{bmatrix} \tag{6}$$

In Eq. (6), $c_\Omega := \cos(\Omega t)$ and $s_\Omega := \sin(\Omega t)$. Hereafter the subscript i denotes an initial state. Equation (5) is simplified as

$$x(t) = -a\cos(\Omega t + \phi) + \frac{2b}{\Omega} \tag{7}$$

$$y(t) = 2a\sin(\Omega t + \phi) - 3bt + d \tag{8}$$

$$\dot{x}(t) = \Omega a\sin(\Omega t + \phi) \tag{9}$$

$$\dot{y}(t) = 2\Omega a\cos(\Omega t + \phi) - 3b \tag{10}$$

where

$$a := \sqrt{(3x_i + 2\dot{y}_i/\Omega)^2 + (\dot{x}_i/\Omega)^2} \tag{11}$$

$$b := 2\Omega x_i + \dot{y}_i \tag{12}$$

$$d := y_i - 2\dot{x}_i/\Omega \tag{13}$$

$$\phi := \arctan\left(\frac{\dot{x}_i}{\Omega(3x_i + 2\dot{y}_i/\Omega)}\right) \tag{14}$$

Since the follower position forms

$$\left(\frac{x - 2b/\Omega}{a}\right)^2 + \left(\frac{y + 3bt - d}{2a}\right)^2 = 1 \tag{15}$$

the relative motion of the follower represents an elliptic orbit at $b = 0$ and a leader-centered ellipse at $b = d = 0$. Thus the constants a, b, d, and ϕ denote the size of the relative orbit, the drift velocity, the center distance of the ellipse from the leader satellite, and the initial phase, respectively.

2.2. Modal equations

A variable transformation based on modal analysis can simplify the relative motion of the follower satellite [18, 23]. The system matrix A for the in-plane motion of the HCW equations is defective and only three eigenvectors and eigenvalues are obtained, although the order of A is four. The eigenvectors and eigenvalues are calculated as

$$\left[\begin{array}{ccc} \boldsymbol{e}_1 & \boldsymbol{e}_3 & \boldsymbol{e}_4 \end{array} \right] = \left[\begin{array}{ccc} 0 & -1/2 & -1/2 \\ 0 & j/2 & -j/2 \\ 1 & j & -j \\ 0 & 1 & 1 \end{array} \right] \tag{16}$$

$$\lambda_1 = 0, \qquad \lambda_3 = -j\Omega, \qquad \lambda_4 = j\Omega \tag{17}$$

where j is an imaginary number. The following manipulations give two real eigenvectors:

$$\begin{aligned} \boldsymbol{e}_3' &= (\boldsymbol{e}_3 - \boldsymbol{e}_4)/j \\ &= \left[\begin{array}{cccc} 0 & 1 & 2 & 0 \end{array} \right]^T \end{aligned} \tag{18}$$

$$\begin{aligned} \boldsymbol{e}_4' &= (\boldsymbol{e}_3 + \boldsymbol{e}_4) \\ &= \left[\begin{array}{cccc} -1 & 0 & 0 & 2 \end{array} \right]^T \end{aligned} \tag{19}$$

The superscript "T" denotes the transpose of a vector or matrix.

A generalized eigenvector $\boldsymbol{e}_2$ is obtained as follows.

$$\begin{aligned} &(A - \lambda_1 I)\, \boldsymbol{e}_2 = \boldsymbol{e}_1 \\ &\Rightarrow \boldsymbol{e}_2 = \left[\begin{array}{cccc} -2/(3\Omega) & 0 & \alpha & 1/\Omega \end{array} \right]^T \end{aligned} \tag{20}$$

In Eq. (20), α is an arbitrary value and henceforth the case for $\alpha = 0$ is considered for simplicity. The modal variables are defined using the transformation matrix that consists of the eigenvectors as

$$\begin{aligned} \boldsymbol{\xi} &= \left[\begin{array}{cccc} \xi_1 & \xi_2 & \xi_3 & \xi_4 \end{array} \right]^T \\ &:= P\boldsymbol{x} \end{aligned} \tag{21}$$

where

$$P := \left[\begin{array}{cccc} -\boldsymbol{e}_4' & \boldsymbol{e}_3' & -\boldsymbol{e}_1 & -3\Omega \boldsymbol{e}_2 \end{array} \right]^{-1} \tag{22}$$

and equivalently,

$$\xi_1 = -3\Omega x - 2\dot{y} \tag{23}$$

$$\xi_2 = \dot{x} \tag{24}$$

$$\xi_3 = 2\dot{x} - \Omega y \tag{25}$$

$$\xi_4 = 2\Omega x + \dot{y} \tag{26}$$

It is noted that the matrix P in Eq. (22) is defined as the inverse of the eigenvectors to simplify the formulation. The modal variables ξ_1 and ξ_2 denote an oscillatory mode, whereas ξ_3 means the distance between the leader and the center of the relative elliptic orbit and ξ_4 is the drift velocity, respectively. In fact, the Euclidean norm of ξ_1/Ω and ξ_2/Ω has the same form as the parameter a shown in Eq. (11); the initial values of $-\Omega\xi_3$ and ξ_4 are equivalent to the parameters d and b defined in Eqs. (13) and (12).

The differential equations of the modal variables are described as follows:

$$\dot{\boldsymbol{\xi}} = PAP^{-1} + PB\boldsymbol{u}_{xy} \tag{27}$$

$$= \begin{bmatrix} 0 & \Omega & 0 & 0 \\ -\Omega & 0 & 0 & 0 \\ 0 & 0 & 0 & 3\Omega \\ 0 & 0 & 0 & 0 \end{bmatrix} \boldsymbol{\xi} + \begin{bmatrix} 0 & -2 \\ 1 & 0 \\ 2 & 0 \\ 0 & 1 \end{bmatrix} \boldsymbol{u}_{xy} \tag{28}$$

The state transition matrix Φ is also simplified with the modal variables as:

$$P\Phi P^{-1} = \begin{bmatrix} \cos(\Omega t) & \sin(\Omega t) & 0 & 0 \\ -\sin(\Omega t) & \cos(\Omega t) & 0 & 0 \\ 0 & 0 & 1 & 3\Omega t \\ 0 & 0 & 0 & 1 \end{bmatrix} \tag{29}$$

Equations (28) and (29) indicate that the oscillatory mode described with ξ_1 and ξ_2 are decoupled with the drift motion terms ξ_3 and ξ_4.

2.3. Rotational equations

The rotational motion of the follower is discussed under the assumption that z_b-axis in the follower-fixed frame corresponds with the z-axis. The rotational equations of motion of the follower in the x–y plane is expressed with a single spin motion around the z-axis as

$$\dot{\psi} = \omega_z - \Omega \tag{30}$$

$$J_z\dot{\omega}_z = T_z \tag{31}$$

where ψ, ω_z, T_z, and J_z are the attitude angle of the follower in the leader-fixed frame, the angular rate, the external torque generated with the thrusters, and the moment of inertia around the z_b-axis of the follower-fixed frame, respectively.

In the present paper, the follower satellite is assumed to equip two body-fixed thrusters for position and attitude control and the x_b-axis of the body-fixed frame corresponds with the thrust direction as shown in Fig. 1. The thrusters can generate variable magnitudes of thrust forces whose directions are restricted only in positive direction due to thruster mechanisms. Thus the external accelerations shown in Eq. (4) are written as

$$\boldsymbol{u}_{xy} = \frac{1}{m} R(\psi)\boldsymbol{F}_b \tag{32}$$

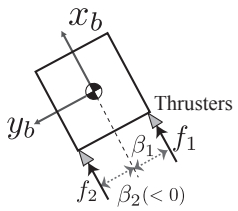

Figure 1: Thruster configuration.

where m and $\boldsymbol{F}_b = \left[\begin{array}{cc} f_1 + f_2 & 0 \end{array} \right]^T$ $(f_1, f_2 \geq 0)$ are the satellite mass and the thruster force vector in the body-fixed frame, respectively, and $R(\cdot)$ denotes a rotational matrix around the z_b-axis, that is,

$$R\left(\psi\right) = \left[\begin{array}{cc} \cos\psi & \sin\psi \\ -\sin\psi & \cos\psi \end{array} \right] \tag{33}$$

The control torque is written as

$$T_z = f_1\beta_1 + f_2\beta_2 \tag{34}$$

where β_1 and β_2 are the moment arms of each thruster; note that β_i is defined in this study to take a negative value in the case that the thruster generates a clockwise directional control torque.

Consequently, the following relation is used to distribute the required control acceleration and torque into the two thrusters.

$$\left[\begin{array}{c} f_1 \\ f_2 \end{array} \right] = \left[\begin{array}{cc} 1 & 1 \\ \beta_1 & \beta_2 \end{array} \right]^{-1} \left[\begin{array}{c} m\sqrt{u_x^2 + u_y^2} \\ T_z \end{array} \right] \tag{35}$$

Although the inverse matrix in the right-hand side of Eq. (35) becomes singular at $\beta_1 = \beta_2$, this singularity can be ignored because such condition occurs in which the two thrusters generate control torques in the same direction; in that case the system becomes uncontrollable.

2.4. Attitude constraints

In a reconfiguration maneuver, the size of the relative orbit is controlled to that of a desired relative orbit, which is described in terms of the modal variables as $(\xi_{1i}, \xi_{2i}, \xi_{3i}, \xi_{4i}) \rightarrow (\xi_{1d}, \xi_{2d}, \xi_{3i}, \xi_{4i})$. In addition, the maneuver aims to orient a specific direction of the follower, e.g., the normal direction of solar array panels or a telescope. Such inertially-oriented constraint arises from mission requirements; obtaining solar energy or sun observation [24]. As shown in Fig. 2, this paper assumes that the desired direction as X-axis in the inertial frame, and the specific direction to be oriented is denoted with ψ_{offset} in the body-fixed frame. The attitude angle to be oriented along the X-axis is represented in the inertial frame:

$$\Psi(t) := \theta(t) + \psi(t) + \psi_{\text{offset}} \tag{36}$$

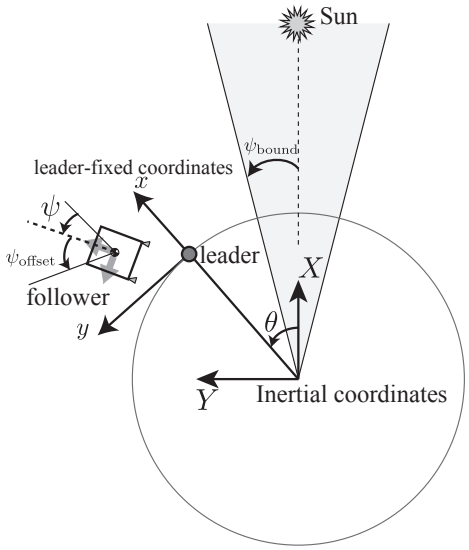

Figure 2: Attitude constraint in the inertial coordinate system.

where θ denotes the true anomaly of the leader satellite. Therefore the attitude constraint considered in this study is keeping the attitude angle Ψ around the X-axis throughout the maneuver: that is, the angle ψ_{bound} in Fig. 2 should be bounded.

3. Control Method

In this section, an attitude tracking controller to orient the thrust direction along desired one is firstly derived because only two thrusters are available for a formation reconfiguration. The attitude controller enables considering the control inputs for the reconfiguration maneuver as accelerations. Thus, for the tracking controller, Subsection 3.2 shows optimal reconfiguration inputs in terms of the accelerations. Then, boundary conditions that make the input trajectory an ellipse are derived in Subsection 3.3, which enables bounding the attitude angle around the desired direction. Furthermore, Subsection 3.4 shows that the initial input angle can be oriented into the desired direction by properly setting maneuver terminated time, and the estimation method of the maximum attitude bound is described in Subsection 3.5.

3.1. Reference acceleration tracking

An attitude control method using the body-fixed thrusters is derived for tracking desired thrust directions. Since the follower satellite equips only two thrusters, the follower's attitude must be controlled so that the thrust direction is oriented along the desired acceleration direction. In other words, for an arbitrary reference acceleration $(u_{xd}(t), u_{yd}(t))$ and its angle $\psi_d(t) := \arctan\left(u_{yd}(t)/u_{xd}(t)\right)$, the attitude control to realize $\psi(t) \to \psi_d(t)$ is needed. To this end, the following Lyapunov function candidate is adopted.

$$L = \frac{1}{2}(\psi - \psi_d)^2 + \frac{1}{2}\left(\dot{\psi} - \dot{\psi}_d\right)^2 \tag{37}$$

The time derivative of Eq. (37) is calculated as

$$\begin{aligned}\dot{L} &= \left(\dot{\psi} - \dot{\psi}_d\right)\left(\ddot{\psi} - \ddot{\psi}_d + \psi - \psi_d\right) \\ &= \left(\dot{\psi} - \dot{\psi}_d\right)\left(T_z/J_z - \ddot{\psi}_d + \psi - \psi_d\right)\end{aligned} \tag{38}$$

Thus the following controller is proposed.

$$T_z/J_z = \ddot{\psi}_d - \psi + \psi_d - K_\psi(\dot{\psi} - \dot{\psi}_d) \tag{39}$$

where K_ψ is a positive constant gain. Substituting this control input into Eq. (38), we obtain the time derivative of the Lyapunov function as

$$\dot{L} = -K_\psi\left(\dot{\psi} - \dot{\psi}_d\right)^2 < 0 \tag{40}$$

The control torque shown in Eq. (39) therefore enables the follower attitude to track the reference acceleration angle. This indicates that the reconfiguration problem under the attitude constraint can be dealt with as the reconfiguration under the directional constraint of the reference accelerations. Henceforth, the attitude constraint is interchangeably denoted as the input directional constraints under the reference acceleration tracking.

Note that the reference inputs u_{xd} and u_{yd} must be at least two times differentiable due to the term $\ddot{\psi}_d$ in Eq. (39). If the reference inputs include a feedback term of the velocity $\dot{x}$, the reference inputs require the term $\ddot{\psi}_d$ for the feedback that results in the time derivative of acceleration $\dddot{x}$. Such term is difficult to estimate and thus full-state feedback controllers, e.g., linear-quadratic regulator, are not applicable to design the reference accelerations in this study.

3.2. Reference optimal controller

The optimal controller design for the reference inputs under the input directional constraint is shown on the basis of the method in [11]. The advantages of using the controller are: 1) the optimal inputs are infinitely differentiable because of a series of time function; 2) the analytical expression of the controller provides a clue for conditions which satisfy the constraint on the input direction. The control method in [11] is briefly followed in this subsection.

Regarding accelerations as control inputs, an optimal reconfiguration controller is designed to minimize the energy consumption of the maneuver. A cost function is defined for the maneuver with a terminated time t_f as follows.

$$J = \int_{t_0}^{t_f} \left(u_x^2 + u_y^2\right) \mathrm{d}t \tag{41}$$

where t_0 is maneuver starting time. The control inputs are described with the Fourier series for representing arbitrary inputs as:

$$u_x = \frac{a_{x0}}{2} + \sum_{n=1}^{\infty} \left(a_{xn} \cos\left(\frac{2n\pi}{\Delta t} t\right) + b_{xn} \sin\left(\frac{2n\pi}{\Delta t} t\right) \right) \tag{42}$$

$$u_y = \frac{a_{y0}}{2} + \sum_{n=1}^{\infty} \left(a_{yn} \cos\left(\frac{2n\pi}{\Delta t} t\right) + b_{yn} \sin\left(\frac{2n\pi}{\Delta t} t\right) \right) \tag{43}$$

where $\Delta t := t_f - t_0$ and a_{k0}, a_{kn}, and b_{kn} $(k = x, y)$ are the Fourier coefficients. The cost function is rewritten in terms of the Fourier coefficients using the Parseval's theorem [25] as follows.

$$J = \frac{\Delta t}{2} \left(\frac{a_{x0}^2}{2} + \sum_{n=1}^{\infty} \left(a_{xn}^2 + b_{xn}^2 \right) \right) + \frac{\Delta t}{2} \left(\frac{a_{y0}^2}{2} + \sum_{n=1}^{\infty} \left(a_{yn}^2 + b_{yn}^2 \right) \right) \tag{44}$$

Thus the optimal control problem is equivalent to finding the Fourier coefficients that minimize the cost function.

The analytical solutions of the HCW equations including control inputs are described as

$$\boldsymbol{x}_f = \boldsymbol{x}_{hf} + \boldsymbol{x}_{pf} \tag{45}$$

$$= \Phi_f \boldsymbol{x}_0 + \boldsymbol{x}_{pf} \tag{46}$$

where the subscripts "h" and "p" denote a homogeneous solution and a particular solution. The subscripts "0" and "f" mean the state when $t = t_0$ and $t = t_f$, respectively. The particular solution is written as a matrix form:

$$\boldsymbol{x}_{pf} = \begin{bmatrix} 2 & -2 & 0 & 0 \\ 0 & 0 & 2 & 0 \\ -3\Omega\Delta t & 0 & 4 & 3 \\ -3 & 4 & 0 & 0 \end{bmatrix} \begin{bmatrix} I_2 \\ I_3 \\ I_4 \\ I_5 \end{bmatrix} \tag{47}$$

$$\Rightarrow \boldsymbol{x}_{pf} = B_p \boldsymbol{I} \tag{48}$$

where

$$I_2 = \int_{t_0}^{t_f} u_y(\tau)\, \mathrm{d}\tau \tag{49}$$

$$I_3 = \int_{t_0}^{t_f} u_y(\tau) \cos\left[\Omega(\Delta t - \tau)\right] \mathrm{d}\tau - \int_{t_0}^{t_f} u_x(\tau) \sin\left[\Omega(\Delta t - \tau)\right] \mathrm{d}\tau \tag{50}$$

$$I_4 = \int_{t_0}^{t_f} u_y(\tau) \sin\left[\Omega(\Delta t - \tau)\right] \mathrm{d}\tau + \frac{1}{2} \int_{t_0}^{t_f} u_x(\tau) \cos\left[\Omega(\Delta t - \tau)\right] \mathrm{d}\tau \tag{51}$$

$$I_5 = \Omega \int_{t_0}^{t_f} u_y(\tau)\, \tau \mathrm{d}\tau - \int_{t_0}^{t_f} \frac{2}{3} u_x(\tau)\, \mathrm{d}\tau \tag{52}$$

These integral terms describe the constraints between a desired state and a homogeneous solution as

$$\begin{aligned}\boldsymbol{I} &= B_p^{-1}\left(\boldsymbol{x}_f - \boldsymbol{x}_{hf}\right) \\ &= \begin{bmatrix} 2 & 0 & 0 & 1 \\ 3/2 & 0 & 0 & 1 \\ 0 & 1/2 & 0 & 0 \\ 2\Omega\Delta t & -2/3 & 1/3 & \Omega\Delta t \end{bmatrix} \begin{bmatrix} \Omega\left(x_f - x_{hf}\right) \\ \dot{x}_f - \dot{x}_{hf} \\ \Omega\left(y_f - y_{hf}\right) \\ \dot{y}_f - \dot{y}_{hf} \end{bmatrix}\end{aligned} \tag{53}$$

These boundary constraints are transformed in terms of the modal variables as follows.

$$\begin{aligned}\boldsymbol{I}_\xi &= \begin{bmatrix} I_{\xi_2} & I_{\xi_3} & I_{\xi_4} & I_{\xi_5} \end{bmatrix}^T \\ &:= B_p^{-1} P^{-1}\left(\boldsymbol{\xi}_f - \boldsymbol{\xi}_h\right)\end{aligned} \tag{54}$$

The permutation of the components of $\boldsymbol{I}_\xi$ defines $\boldsymbol{I}'_\xi := \begin{bmatrix} I_{\xi_3} & I_{\xi_4} & I_{\xi_5} & I_{\xi_2} \end{bmatrix}^T$ and the boundary constraints are further transformed as

$$\boldsymbol{K} = \begin{bmatrix} \cos\frac{\beta}{2} & \sin\frac{\beta}{2} & 0 & 0 \\ -\sin\frac{\beta}{2} & \cos\frac{\beta}{2} & 0 & 0 \\ 0 & 0 & -\frac{2}{\beta} & 1 \\ 0 & 0 & 0 & 1 \end{bmatrix} \boldsymbol{I}'_\xi \tag{55}$$

where $\boldsymbol{K} = \begin{bmatrix} K_3 \sin(\beta/2) & K_4 \sin(\beta/2) & K_5 & K_2 \end{bmatrix}^T$ and $\beta = \Omega\Delta t$. The transformed constraints $\boldsymbol{K}$ provide simple relations with Lagrange multipliers as shown in [23] and the multipliers are analytically solved for satisfying the boundary constraints [11]. The resulting optimal inputs for the fixed time reconfiguration maneuver are described as follows.

$$u_x(t) = \frac{2}{3}T_1 + \frac{\Lambda}{2}\sin(\Omega\left(t - t_0\right) - \Theta) \tag{56}$$

$$u_y(t) = T_0 - T_1\Omega\left(t - t_0\right) + \Lambda\cos(\Omega\left(t - t_0\right) - \Theta) \tag{57}$$

where T_0, T_1, Λ, and Θ are constants described with the Lagrange multipliers [11].

3.3. Elliptic input trajectory

The analytical expression of the optimal controller gives us a clue for satisfying the input directional constraint. The controller shown in Eqs. (56) and (57) has the same form as the analytical solutions of the HCW equations in Eqs. (7) and (8), and this fact indicates that the input trajectory becomes an ellipse at $T_1 = 0$ and furthermore an origin-centered ellipse at $T_0 = T_1 = 0$. Such elliptic input trajectory can change the acceleration angle along with the input directional constraint, because both the acceleration angle and desired one represented in the leader-fixed frame vary monotonically. In fact, the average rate of the acceleration angle changes is Ω as shown in Eqs. (56) and (57) and the desired angle represented in the leader-fixed frame also varies at the rate Ω due to the leader's circular orbit. Thus if the initial input direction is within allowable directions, the difference between the input angle and desired one is expected to be bounded.

In order to realize the elliptic input trajectory, conditions for satisfying $T_1 = 0$ are sought. The constant T_1 is described with the Lagrange multipliers and they are related to the boundary states of the follower, i.e., the initial and final states when the maneuver is implemented. The constant T_1 is written as [11]

$$T_1 = \frac{\lambda_5 (\beta, K_4, K_5)}{\beta} \tag{58}$$

The variable λ_5 is the Lagrange multiplier described as

$$\lambda_5 = \frac{1}{D}\left[\frac{1}{2\Omega}\left(\frac{\beta - \sin\beta}{1-\cos\beta} + \frac{1}{4}\frac{\beta+\sin\beta}{1-\cos\beta}\right)K_5 - \frac{2}{\beta\Omega}\left(\frac{\beta}{2}\cot\frac{\beta}{2} - 4/3\right)K_4\right] \tag{59}$$

where

$$D = \frac{1}{6\Omega^2}\left[\frac{\beta-\sin\beta}{1-\cos\beta} + \frac{1}{4}\frac{\beta+\sin\beta}{1-\cos\beta}\right]\left(\frac{\beta}{2} + \frac{8}{3\beta}\right) - \frac{4}{\beta^2\Omega^2}\left(\frac{\beta}{2}\cot\frac{\beta}{2} - \frac{4}{3}\right)^2 \tag{60}$$

Since the boundary states of ξ_3 and ξ_4 are $\xi_{3,0} = \xi_{3hf}$ and $\xi_{4,0} = \xi_{4hf}$ for the reconfiguration maneuver, the constraints $\boldsymbol{K}$ are simplified to $K_2 = K_5 = 0$ from Eqs. (54) and (55). As a result, the condition $T_1 = 0$ is equivalent to $K_4 = 0$ from Eqs. (58) and (59).

Using Eqs. (54) and (55), we obtain the condition on the boundary states for satisfying $K_4 = 0$ as follows.

$$(\xi_{1f} - \xi_{1hf}) + (\xi_{2f} - \xi_{2hf})\cot\left(\frac{\beta}{2}\right) = 0 \tag{61}$$

The modal variables are rewritten with polar coordinates as

$$\xi_{1f} = a_f \cos\gamma_f \tag{62}$$
$$\xi_{2f} = a_f \sin\gamma_f \tag{63}$$

Note that, since $a_f = \sqrt{\xi_{1f}^2 + \xi_{2f}^2}$, the variable a_f indicates the size of the relative orbit at the terminated time t_f. The homogeneous solutions of the modal variables are described using the state transition matrix in Eq. (29) as follows.

$$\xi_{1hf} = a_0\cos\gamma_0\cos\beta + a_0\sin\gamma_0\sin\beta \tag{64}$$
$$\xi_{2hf} = -a_0\cos\gamma_0\sin\beta + a_0\sin\gamma_0\cos\beta \tag{65}$$

Substitution of Eqs. (62)-(65) into Eq. (61) and the assumption $\cot(\beta/2) \neq 0$ yield

$$(a_f\cos\gamma_f - a_0\cos(\gamma_0-\beta))\tan\left(\frac{\beta}{2}\right) + a_f\sin\gamma_f - a_0\sin(\gamma_0-\beta) = 0 \tag{66}$$

$$\Rightarrow a_f\left(\tan\left(\frac{\beta}{2}\right)\cos\gamma_f + \sin\gamma_f\right) - a_0\left(\sin(\gamma_0-\beta) + \tan\left(\frac{\beta}{2}\right)\cos(\gamma_0-\beta)\right) = 0 \tag{67}$$

In the above equations, a_f and a_0 are nonzero values for the reconfiguration maneuver and Eq. (67) is equivalent to the following conditions:

$$\tan\left(\frac{\beta}{2}\right)\cos\gamma_f + \sin\gamma_f = 0 \tag{68}$$

$$\sin(\gamma_0 - \beta) + \tan\left(\frac{\beta}{2}\right)\cos(\gamma_0 - \beta) = 0 \tag{69}$$

These equations hold at

$$\gamma_f = -\frac{\beta}{2} \tag{70}$$

$$\gamma_0 = \frac{\beta}{2} \tag{71}$$

From the definitions of γ_f, γ_0, ξ_1, and ξ_2, Eqs. (70) and (71) are described as the boundary conditions of the follower position:

$$\frac{y_f}{2x_f} = \tan\left(-\frac{\beta}{2}\right) \tag{72}$$

$$\frac{y_0}{2x_0} = \tan\left(\frac{\beta}{2}\right) \tag{73}$$

Therefore by setting the initial and final position of the follower to satisfy Eqs. (72) and (73), the condition $T_1 = 0$ holds. That is, the resulting optimal input trajectory in Eqs. (56) and (57) becomes an ellipse.

3.4. Initial input angle

As discussed in the previous subsection, the elliptic input trajectory can bound the difference between the acceleration angle and desired one if the initial input angle is coincident with the desired angle. The initial acceleration angle when the maneuver starts is obtained by substituting $t = t_0$ into Eqs. (56) and (57) as

$$\psi_{d0} = \arctan\left(\frac{2\left(T_0 + \Lambda\cos\left(-\Theta\right)\right)}{\Lambda\sin\left(-\Theta\right)}\right) \tag{74}$$

On the other hand, since the attitude angle ψ is controlled to ψ_d by using the attitude tracking controller, the initial angle ψ_{d0} is described from Eq. (36) as

$$-\psi_{d0} = \Omega t_0 + \psi_{\text{offset}} \tag{75}$$

where, without loss of generality, the initial state $\boldsymbol{x}_i$ is assumed to be on the X-axis, i.e., $\theta(t_i) = 0$. The maneuver starting time t_0 is determined with Eq. (73) and is written in terms of the initial position of the follower (i.e., when $\theta = 0$) as follows.

$$\frac{\beta}{2} = \arctan\left(\frac{y_i}{2x_i}\right) - \Omega t_0 \tag{76}$$

Substituting Eq. (76) into Eq. (75) provides

$$\psi_{d0} - \frac{\beta}{2} = -\arctan\left(\frac{y_i}{2x_i}\right) - \psi_{\text{offset}} \tag{77}$$

The left-hand side of Eq. (77) is the function of the terminated time t_f because the initial acceleration angle ψ_{d0} can vary according to the final time t_f. Equation (77) thus determines the proper final time t_f that can realize the initial acceleration angle to coincide with the desired one. In addition, Eq. (77) has multiple solutions as $t_f + 2N\pi/\Omega$ $(N = 0, 1, 2, ...)$ because the relative motion of the follower is periodic. Note that, although the terms $\psi_{d0} - \beta/2$ vary depending on t_f, Eq. (77) may not have a solution for a certain range of ψ_{offset}. However, in that case, relaxing the condition in Eq. (75) to

$$-\psi_{d0} \leq |\Omega t_0 + \psi_{\text{offset}} \pm \Gamma| \tag{78}$$

where Γ is an initial error with respect to the desired angle, we can find the solution of the terminated time t_f.

3.5. Maximum bound estimation

The maximum bound of the input angle with respect to the desirable angle needs to be numerically obtained because they do not strictly coincide throughout the reconfiguration maneuver, even though the initial acceleration angle can be oriented along the desirable one. This stems from the elliptic motion of the acceleration trajectory, whereas the desired angle change is a circular motion.

Despite the fact that $\Psi(t)$ in Eq. (36) is expressed with the analytical form, its extremum values may not be analytically obtained due to the nonlinearity of ψ_d (equivalent to ψ). Their estimated values, however, are easily obtained by solving $\dot{\Psi}(t) = 0$ under the assumption $T_0 \coloneqq 0$: the condition $\dot{\Psi}(t) = 0$ holds at

$$t - t_0 = \frac{2\Theta + \arccos(-1/3)}{2\Omega}, \quad -\frac{-2\Theta + \arccos(-1/3)}{2\Omega} \tag{79}$$

The assumption $T_0 \coloneqq 0$ does not hold except for special cases of boundary conditions though, the approximate solutions in Eq. (3.5) provide good estimations for the maximum bound of the attitude angle as demonstrated in the following section. Furthermore, the approximate solutions are useful as initial estimations for numerical solvers of nonlinear equations, such as Newton's method. Consequently the accurate maximum bound of the attitude angle can be calculated with low computational efforts using the approximate solutions in Eq. (3.5).

4. Numerical simulation

This section shows numerical simulation results for three cases to demonstrate the effectiveness of the proposed reconfiguration method. A leader satellite is assumed to be orbiting in a circular orbit at 6.313×10^{-4} rad/s. The follower satellite's mass, the moment of inertia, and the moment arm of the thrusters are set to $m = 200$ kg, $J_z = 60$ kgm^2, and

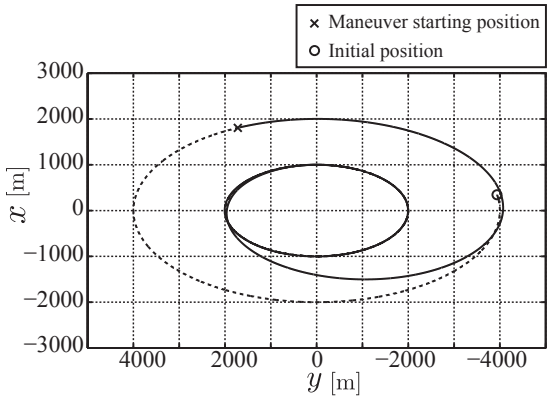

Figure 3: Reconfiguration trajectory of the follower ($\psi_{\text{offset}} = 0$ deg, $t_0 = 7036$ s, $t_f = 18396$ s).

$(\beta_1, \beta_2) = (0.5, -0.5)$ m, respectively, and the initial follower attitude is assumed to coincide with a desired angle with no angular velocity. All simulation cases aim the reconfiguration of the follower from the relative orbit at $a_i = 2000$ m to the target orbit at $a_f = 1000$ m with the initial position $(x_i, y_i) = (347.3, -3939.2)$ m, i.e., $\arctan(y_i/(2x_i)) = -80$ deg.

The first numerical simulation is conducted setting the parameter for the attitude constraint as $\psi_{\text{offset}} = 0$ deg. For this attitude constraint, the terminated time t_f is numerically obtained as $t_f = 18396$ s ($N = 0$) using Eq. (77) and then the starting time of the maneuver is calculated as 7036 s from Eq. (76). Figure 3 describes the reconfiguration trajectory of the follower satellite, in which the dashed and solid line represent the coasting and relocation trajectory of the follower, respectively. The circle and cross indicate the initial and maneuver starting positions. As seen in the Fig. 3, the follower is successfully controlled to the target relative orbit. The time history of the attitude angle with respect to the inertial frame is shown in Fig. 4, and it represents the attitude angle of the follower can be bounded around the X-axis of the inertial frame. The estimated bound of the attitude angle is calculated as 34.4 deg using Eqs. (36) and (3.5), whereas the exact value is found to be 35.2 deg. Thus the maximum bound can be precisely estimated as discussed in the subsection 3.5. In Figs. 5 and 6, the reference acceleration trajectory and the time history of the total thruster forces are shown, respectively. The reference input trajectory in Fig. 5 describes an ellipse as expected in the previous section, and the thruster forces throughout the maneuver in Fig. 6 are kept positive not to violate the constraints on the thruster mechanisms. The numerical simulation result yields the cost function as 2.50×10^{-5} m^2/s^3.

The second simulation is performed with the attitude offset angle $\psi_{\text{offset}} = -30$ deg. The terminated time $t_f = 16699$ s and starting time $t_0 = 8734$ s are obtained from Eqs. (76) and (77), respectively. In Fig. 7, the dashed and solid lines describe the follower coasting and reconfiguration trajectory, respectively, and the relative orbit of the follower is successfully controlled to the desired relative orbit. Figure 8 shows the time history of the attitude angle including the offset angle in the inertial frame. Although the maximum bound is larger than the previous simulation result, the attitude angle with the offset angle ψ_{offset} can be bounded around the X-axis in the inertial frame. The reason of the larger bound is that the center of

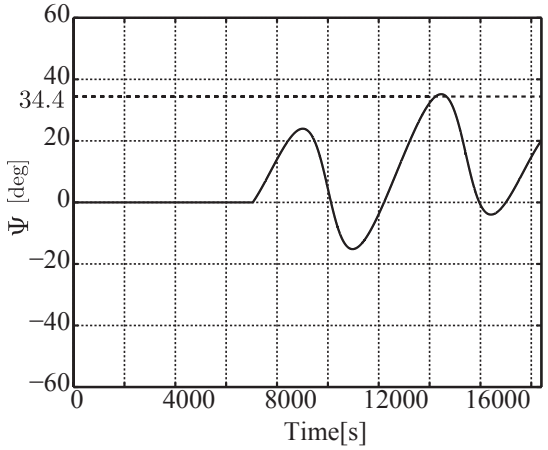

Figure 4: Time history of the attitude angle of the follower in the inertial frame ($\psi_{\text{offset}} = 0$ deg, $t_0 = 7036$ s, $t_f = 18396$ s).

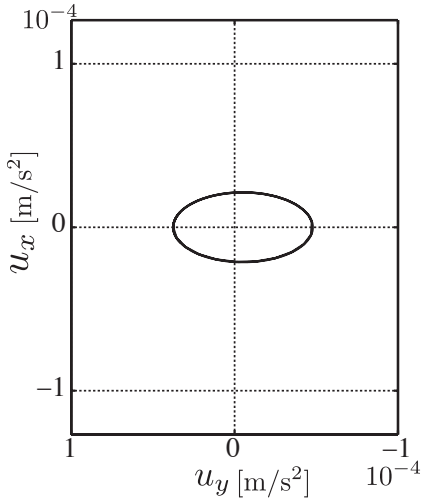

Figure 5: Input trajectory in the leader-fixed frame ($\psi_{\text{offset}} = 0$ deg, $t_0 = 7036$ s, $t_f = 18396$ s).

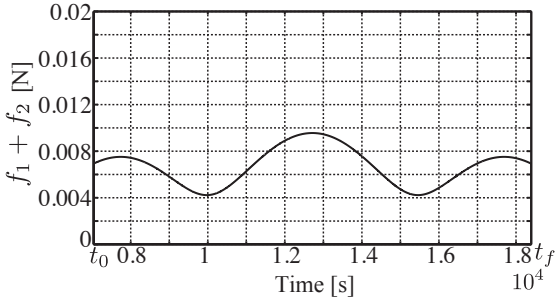

Figure 6: Time history of the total thruster forces ($\psi_{\text{offset}} = 0$ deg, $t_0 = 7036$ s, $t_f = 18396$ s).

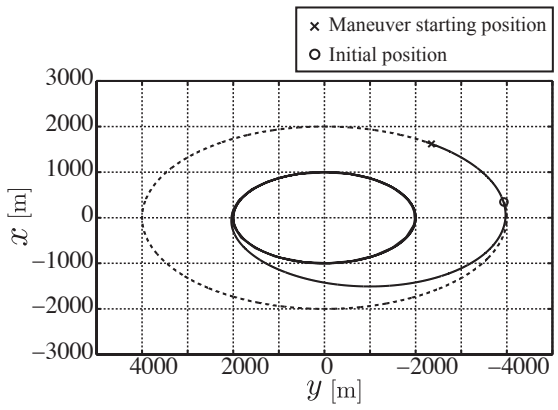

Figure 7: Reconfiguration trajectory of the follower ($\psi_{\text{offset}} = -30$ deg, $t_0 = 8734$ s, and $t_f = 16699$ s).

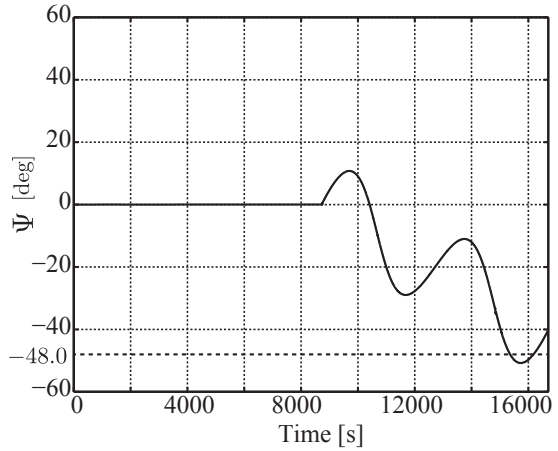

Figure 8: Time history of the attitude angle of the follower in the inertial frame ($\psi_{\text{offset}} = -30$ deg, $t_0 = 8734$ s, and $t_f = 16699$ s).

the elliptic input trajectory in Fig. 9 has a larger offset than that of the previous simulation in Figs. 5. Figure 10 illustrates the time history of the thruster forces and the magnitude of the thrusts is also larger than that of the previous simulation in Fig. 6 because of the shorter maneuver time: $\Delta t = 7965$ s for the second case and $\Delta t = 11900$ s for the first case. The resulting cost function is obtained as $J = 6.77 \times 10^{-5}$ m^2/s^3.

The third simulation result is for the same initial condition and the attitude constraint as the first one except for the terminated time t_f. The terminated time t_f more than one orbital period is set as $t_f = 18396 + 2\pi/\Omega = 28348$ s, whereas the starting time is the same as the first simulation, i.e., and $t_0 = 7036$ s. In Fig. 11, the dashed and solid lines similarly represent the coasting motion and reconfiguration trajectory of the follower, respectively. The relative orbit of the follower is successfully relocated to the desired relative orbit. Figure 12 represents the time history of the attitude angle Ψ in the inertial frame and the attitude angle is kept around the X-axis of the inertial coordinates. As shown in Fig. 13,

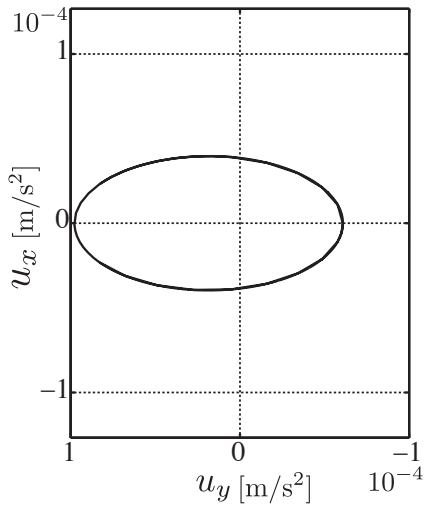

Figure 9: Input trajectory in the leader-fixed frame ($\psi_{\text{offset}} = -30$ deg, $t_0 = 8734$ s, and $t_f = 16699$ s).

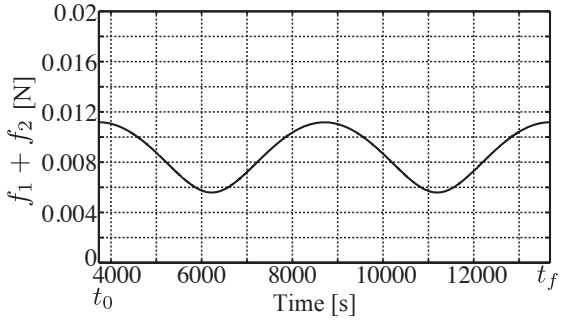

Figure 10: Time history of the total thruster forces ($\psi_{\text{offset}} = -30$ deg, $t_0 = 8734$ s, and $t_f = 16699$ s).

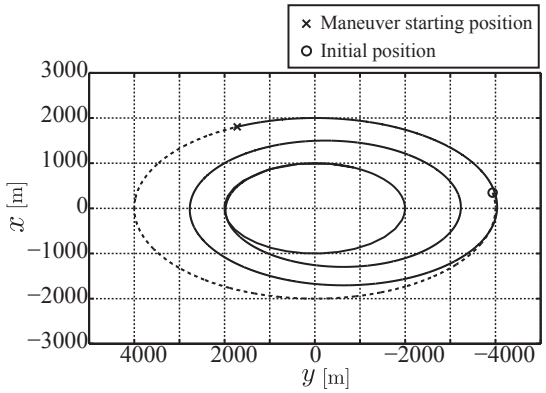

Figure 11: Reconfiguration trajectory of the follower ($\psi_{\text{offset}} = 0$ deg, $t_0 = 7036$ s, and $t_f = 28348$ s).

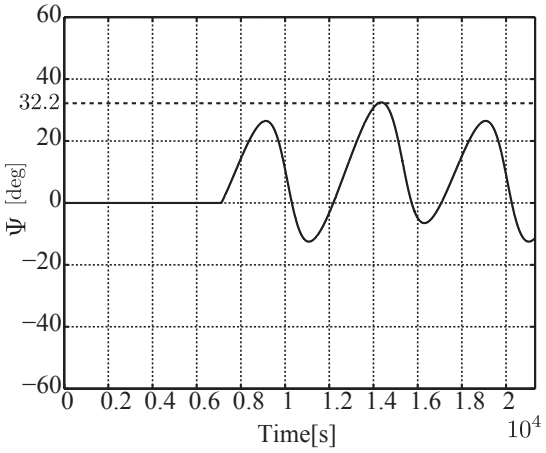

Figure 12: Time history of the attitude angle of the follower in the inertial frame ($\psi_{\text{offset}} = 0$ deg, $t_0 = 7036$ s, and $t_f = 28348$ s).

the thrusters generate positive forces and the resulting cost function for this maneuver is 1.06×10^{-5} m^2/s^3, which is smaller than the previous simulations due to the longer maneuver time.

Table 1 summarizes the maneuver time, the energy consumptions, the estimated maximum bounds of the attitude angle, and their exact values for the three cases. The energy consumption is significantly affected by the maneuver duration Δt: a longer maneuver time can reduce the energy consumption. The maximum bound of the attitude angle is accurately estimated under the assumption $T_0 \fallingdotseq 0$, and more accurate results will be obtained by using nonlinear equation solvers, such as Newton's method.

5. Conclusions

An optimal formation reconfiguration under attitude constraints with respect to an inertial frame has been derived using only two thrusters. To control a follower position and

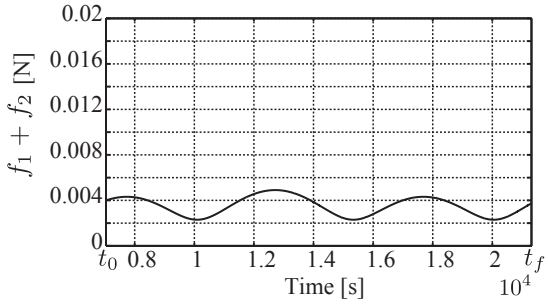

Figure 13: Time history of the total thruster forces ($\psi_{\text{offset}} = 0$ deg, $t_0 = 7036$ s, and $t_f = 28348$ s).

Table 1: Cost function and maximum bound

	first case	second case	third case
maneuver duration, Δt, s	11360	7965	21312
cost function, J, m^2/s^3	2.50×10^{-5}	6.77×10^{-5}	1.06×10^{-5}
estimated maximum bound, deg	34.4	48.0	32.2
exact maximum bound, deg	35.2	50.8	32.4

attitude using the thrusters, an attitude tracking method based on Lyapunov approach has been shown. The tracking controller can reduce the reconfiguration problem under the attitude constraints to the one under thrust directional constraints, which allows us to design the reference inputs in terms of the accelerations. The reference accelerations using the Fourier series reveal that particular boundary conditions can make the input trajectory an ellipse, which can be exploited to satisfy the constraints. Furthermore, the estimation technique for the maximum bound of the attitude angle with respect to the desired direction has been shown. Numerical simulations for three cases have verified the effectiveness of the proposed reconfiguration controller and compared the energy efficiency. Although the proposed reconfiguration maneuver needs to admit the attitude change in some range due to the constraints of the small number of thrusters, the proposed method achieves the optimal formation reconfiguration with bounded and small attitude changes using only few thrusters. Further improvements to overcome the limitation and to involve practical situations such as formation flying in elliptic orbit or under disturbances will be studied in future works.

References

[1] DelpechM, Results of prisma/ffiord extended mission and applicability to future formation flying and active debris removal missions, International Journal of Space Science and Engineering 5 (1(4)) (2013) 382–409.

[2] e. a. Tridon, Daniela Borla, Tandem-x: Dem acquisition in the third year era, International Journal of Space Science and Engineering 5 (1(4)) (2013) 367–381.

[3] L. T. Castellani, S. Llorente, J. M. Fernandez, M. Ruiz, A. Mestreau-Garreau, A. Cropp, A. Santovincenzo, Proba-3 Mission, International Journal of Space Science and Engineering 5 (1(4)) (2013) 349–366.

[4] S. Bandyopadhyay, R. Foust, G. P. Subramanian, S.-J. Chung, F. Y. Hadaegh, Review of Formation Flying and Constellation Missions Using Nanosatellites, Journal of Spacecraft and Rockets 53 (3) (2016) 567–578. doi:10.2514/1.A33291.
URL http://arc.aiaa.org/doi/10.2514/1.A33291
[5] W. H. Clohessy, R. S. Wiltshire, Terminal Guidance System for Satellite Rendezvous, Journal of the Aerospace Sciences 27 (9) (1960) 653–658.
[6] T. J, H. P, Rendezvous with a Target in an Elliptical Orbit, Astronautica Acta 11 (2) (1965) 104–109.
[7] M. Shibata, A. Ichikawa, Orbital Rendezvous and Flyaround Based on Null Controllability with Vanishing Energy, J. Guidance 30 (4) (2007) 934–945.
[8] T. Carter, J. Brient, Fuel-optimal rendezvous for linearized equations of motion, Journal of Guidance Control Dynamics 15 (6) (1992) 1411–1416.
[9] B. S. Kumar, A. Ng, Time-Optimal Low-Thrust Formation Maneuvering Using a Hybrid Linear/Nonlinear Controller, J. Guidance 32 (1) (2009) 343–347.
[10] T. E. Carter, C. J. Pardis, Optimal power-limited rendezvous of a spacecraft with upper and lower bounds on thrust, Proceedings of the AAS/AIAA Astrodynamics Conference (1996) 2183–2210.
[11] P. Palmer, Optimal relocation of satellites flying in near-circular-orbit formations, J. Guidance 29 (3) (2006) 519–526.
[12] H. Cho, S.-Y. Park, H.-E. Park, K.-H. Choi, Analytic Solution to Optimal Reconfigurations of Satellite Formation Flying in Circular Orbit under Perturbation, Aerospace and Electronic Systems, IEEE Transactions on 48 (3) (2012) 2180–2197.
[13] H. Cho, S.-Y. Park, S.-M. Yoo, K.-H. Choi, Analytical solution to optimal relocation of satellite formation flying in arbitrary elliptic orbits, Aerospace Science and Technology (2012) 1–16.
[14] J. Li, X.-N. XI, Fuel-Optimal Low-Thrust Reconfiguration of Formation- Flying Satellites via Homotopic Approach, J. Guidance 35 (6) (2012) 1709–1717.
[15] S. Mitani, H. Yamakawa, Novel Nonlinear Rendezvous Guidance Scheme Under Constraints on Thrust Direction, J. Guidance 34 (6) (2011) 1656–1671.
[16] J. W. Curtis, R. W. Beard, Satisficing: A New Approach to Constructive Nonlinear Control, IEEE Trans. Automat. Contr. 49 (7) (2004) 1090–1102.
[17] S. Mitani, H. Yamakawa, Continuous-Thrust Transfer with Control Magnitude and Direction Constraints Using Smoothing Techniques, J. Guidance 36 (1) (2013) 163–174.
[18] M. Guelman, K. Schilling, D. L. Barnett, Formation flight line of sight guidance, Acta Astronautica 71 (2012) 163–169.
[19] R. Haghighi, C. K. Pang, Concurrent attitude-position control of under-actuated nanosatellites for formation flying, Vol. 2016-July, 2016, pp. 1014–1019. doi:10.1109/ICCA.2016.7505413.
[20] M. Massari, M. Zamaro, Application of SDRE technique to orbital and attitude control of spacecraft formation flying, Acta Astronautica 94 (1) (2014) 409–420. doi:10.1016/j.actaastro.2013.02.001.
URL http://dx.doi.org/10.1016/j.actaastro.2013.02.001
[21] H. Dong, Q. Hu, G. Ma, Dual-quaternion based fault-tolerant control for spacecraft formation flying with finite-time convergence, ISA Transactions 61 (2014) 87–94. doi:10.1016/j.isatra.2015.12.008.
URL http://dx.doi.org/10.1016/j.isatra.2015.12.008
[22] R. Sanchez-Maestro, A. Agenjo-Diaz, A. Cropp, PROBA-3 Formation Flying High Performance Control , in: 5th International Conference on Spacecraft Formation Flying Missions and Technologies, 2013.
[23] P. Palmer, Reachability and Optimal Phasing for Reconfiguration in Near-Circular Orbit Formations, J. Guidance 30 (5) (2007) 1542–1546.
[24] J. S. Llorente, A. Agenjo, C. Carrascosa, C. de Negueruela, A. Mestreau-Garreau, A. Cropp, A. Santovincenzo, Proba-3: Precise formation flying demonstration mission, Acta Astronautica 82 (1) (2013) 38–46.
[25] M. L. Boas, Mathematical methods in the physical sciences, John Wiley & Sons, 2006.